Industrial Combustion
Journal of the International Flame Research Foundation
Article number 201618, June 2020
ISSN 2075-3071

RANS and LES of turbulent premixed flame dynamics for gas turbine combustion systems

[1]Naresh K. Aluri, [2,Δ] Siva PR Muppala

[1]ABB Power Grids, Switzerland
[2] School of Engineering and the Environment,
Faculty of Science, Engineering and Computing,
Kingston University, London, SW15 3DW, UK
[Δ]email: s.muppala@kingston.ac.uk

Abstract

Methodical design of gas turbine premixed turbulent combustion systems for fuel flexibility is a necessity for higher efficiency and operational flexibility, due to the use of vast range of fuel types and fuel mixtures. Different fuels/fuel mixtures have different reactivity and varied molecular transport characteristics. The central theme of this paper is numerical investigation of these effects, along with the dynamics of turbulent premixed high-pressure flames. We studied these dominant factors in two different geometrical configurations, a cylindrical dump combustion system and an industrial gas turbine single burner combustion system.
Here, we chose the algebraic flame surface density model as subgrid scale reaction closure for LES approach in conjunction with three widely employed turbulence models for dump combustor (F-1 configuration). For the second, the flame stability of a swirl burner with mixing section (F-2 configuration) for variation of fuel types is analysed in RANS for two different fuel profiles, a uniform fuel profile and rich core-lean outer. We investigated flame dynamics in conjunction with the vortex breakdown point. This phenomenon is visualized in the context of the Lewis number variation for the rich core-lean outer.

Numerical validation with available experiments are made for two main combustion quantities, flame brush thickness and mean flame position for the dump combustion system. For the swirl burner, only the numerical results are presented with potential reasoning for change of flame stabilization location for variation of Lewis number (for higher hydrocarbons) in the case of rich core-lean outer profile.

Keywords: Turbulent premixed combustion, dynamic flames, the Lewis number, high operating pressures, RANS, LES, Stationary gas turbines

1. Introduction

With the growing expectations on fuel flexibility and improved component life time, design of combustion systems become more complex. Considering the complex phenomena involved in premixed turbulent flames, handling difficulties and economical aspects in conducting experiments, numerical combustion has become a more preferred choice and as a supportive tool for combustion system development and optimization.

The motivation for this study is to understand aspects of molecular transport effects on combustion and their practical importance on location of flame stabilization. Flame stabilization location is crucial for mechanical integrity of the fuel injection and combustion systems. Within this subject, we use a validated progress-variable based

Industrial Combustion
Journal of the International Flame Research Foundation
Article number 201618, June 2020
ISSN 2075-3071

reaction closure for turbulent premixed combustion involving several parameters over a broad range of conditions such as fuel type, pressure, geometrical flame configurations, and turbulence levels[1-4]. In previous studies and publications we have demonstrated that the chosen combustion model is capable of predicting flame location for varied fuel types (Lewis number), operating conditions and geometries. Therefore, we employed the Algebraic Flame Surface Wrinkling (AFSW) model for the current investigation. In this study, the reaction closure is used both in RANS and in the context of Large Eddy Simulation (LES). In this article we have extensively studied the variation of pressure on a sudden expansion dump combustor, which has been experimentally investigated at the Paul-Scherrer-Institute in Switzerland [5]. Also, in this study we investigate in RANS the combustion flow dynamics in a variant of a conical gas turbine burner with mixing section[6]. DNS studies by Wang et.al. [7] show that normalized turbulent flame speed increases with turbulent Reynolds number in lean methane/air mixtures up to 20 bar. The reason is attributed to increased small-scale size eddies, increasing turbulent flame area. These findings have perceived benefits in understanding the flame dynamics in real flame configurations that are studied below.

The experimental details of two flame configurations are numbered F-1 for PSI sudden expansion dump combustor and F-2 configuration for a swirl flow burner variant the later have application in gas turbine combustion systems. The details of simulated conditions are tabulated in Tables 1 and 2.

In the F1-configuration, the outer recirculation zones are created by a sudden expansion jet stabilizes the flame. In this, the operating pressure is varied up to 14bar. In this burner, the flow complexity lies with shear-generated turbulence that exceeds the grid-generated turbulence by several folds. Therefore, it is a challenging task for model validation, for both non-reacting and reacting flows against experiments.

In case of F-2, pressures are varied up to 32bar. In this configuration, RANS is chosen for turbulence closure, the algebraic flame surface wrinkling model for the reaction closure. Also, the importance of molecular transport effects on flame stabilization location in conjunction with the Lewis number variation is demonstrated on this configuration.

Chakraborty and Cant [8] show that the effects of Lewis number for four values 0.6 to 1.2 on flame surface density in spherically expanding flames is strongly dominant on normalized turbulent flame area and thus on normalized turbulent flame speed are in corroboration with the model developed in [9].A relatively recent RANS study by Swaminathan group using the flamelet-based approach gives good agreement for temperature and major species, CO and NOx at atmospheric conditions[10].

2. Description of Turbulent Reaction Model

2.1 Reaction Progress Variable Approach

Numerical calculation of turbulent premixed flames is in general a non-trivial task due to the strong interaction between fluid flow, laminar, and turbulent transport and reaction processes. Typically, for non-reacting flows the coupled partial differential equations for the balance of the average of mass, momentum and turbulence parameters are solved, while for the calculation of flames, additional equations for species and energy are included. A common approach for turbulent premixed flames, as noted above, is the use of a mean reaction progress variable $\overline{C}$, describing the probability to find burned gas. The average reaction zone position is described by the increase of this property from 0 in the unburned mixture to 1 in the products. Taking

Industrial Combustion
Journal of the International Flame Research Foundation
Article number 201618, June 2020
ISSN 2075-3071

adiabatic flame conditions (neglecting radiation) and fast reaction, as can be assumed to a first order approximation at least in non-sooting premixed flames, the average temperature and density follow as a function of the reaction progress variable *c*.

For combustion calculations the use of density-weighted (Favre-averaged) properties $\tilde{\varphi} = \overline{\rho\varphi}/\overline{\rho}$ is convenient, (with the decomposition $\varphi = \tilde{\varphi} + \varphi''$), having the advantage that the set of equations for mass and momentum of incompressible flows can be applied for the calculation of reacting flows[11]. For comparative analysis with experiments, the calculated density-weighted results need to be transformed to the Reynolds-averaged quantities in a post-processing step (possible only for *c* not for velocity etc).

The balance equation for the Favre-averaged reaction progress variable *c* – *based on temperature* – is given by

$$\frac{\partial \overline{\rho}\tilde{c}}{\partial t} + \frac{\partial \overline{\rho}\tilde{u}_j\tilde{c}}{\partial x_j} = \frac{\partial}{\partial x_j}\left(\overline{\rho}\widetilde{u_j''c''}\right) + \overline{w}_c$$

where t is the time, x_j and u_j are the coordinates and the flow components, $\overline{\rho}$ is the gas density and $\overline{w}_c$ is the mean reaction source term. This equation requires the modelling of the turbulent transport term (second term on the right hand side), and the mean reaction source term. For the turbulent transport the common turbulent gradient diffusion approach with turbulent kinematic viscosity ν_t and turbulent Schmidt number Sc_t = 0.7 is used

$$\widetilde{u_j''c''} = \frac{\nu_t}{Sc_t}\frac{\partial \tilde{c}}{\partial x_j}$$

In both RANS and LES contexts, the scalar fluxes are closed using the gradient approach. The primary focus of the current work is to develop and test the source term $\overline{\dot{w}}_c$ of the progress variable both in RANS and LES. There exists variety of models to close $\overline{\dot{w}}_c$ deduced from different approaches. The first author has analysed a number of popular combustion models in literature for two different flame configurations[11]. In a similar study, Burke et al. [12]studied various flame speed correlations for high operating pressures

2.2 Reaction Modelling Approaches

In general, the chemical and hydrodynamic structure of a stretched laminar premixed flame can be preserved in a turbulent flow field over a range of conditions collectively known as the flamelet regime, and the premixed combustion in most of the practical devices falls within the domain of this regime. The major assumption in the laminar flamelet concept as applied to the turbulent premixed flames is that the flame front behaves as a constant-property passive scalar surface, and an increase in the wrinkled flame surface area with increasing turbulence intensity is the dominant mechanism for the observed flame velocity enhancement. For high Damköhler number Da, a premixed flame consists of reactants and products separated by thin laminar flamelets. Since the instantaneous behaviour of these thin layers is same as those of laminar flames, turbulent flame speed s_T can be approximated by the product of the flamelet surface

Industrial Combustion
Journal of the International Flame Research Foundation
Article number 201618, June 2020
ISSN 2075-3071

area and laminar flame speed s_{L0} corrected for the effect of stretch and flame curvature by I_0 and the reaction rate is expressed as

$$\bar{\dot{w}}_c = \rho_u s_{L0} I_0 \Sigma$$

where, ρ_u is the reactant unburned density, s_{L0} the unstretched laminar flame speed, I_0 is the mean stretch factor. In this study, I_0 is normally set to 1.0. Modelling Σ, the flame surface density is the essential part of turbulent premixed flamelet models.
One major advantage of this approach is in decoupling chemistry from the flame-turbulence interaction described by Σ (flame surface-to-volume ratio), ρ_u is the unburned gas density and the factor I_0 includes the effects of flame stretch [13].

Several reaction models exist in the literature, are derived based on physical argumentation for e.g., [14], or through phenomenological approaches. Here, only the ones relevant to this study are partially addressed, while the associated model development issues are discussed in detail.

2.3 Algebraic Flame Surface Wrinkling (AFSW) model

Following the algebraic approach, the flame surface density may be modelled with an algebraic relation for the flame-surface-wrinkling factor $A_T / \bar{A}$, the ratio of turbulent flame surface per unit volume A_T to its projection on its average surface per unit volume $\bar{A}$

$$\Sigma = \frac{A_T}{\bar{A}}$$

In the definition of the reaction rate, the product of stretch factor I_0 and Σ is equated to gradient of the reaction progress variable $|\nabla \tilde{c}|$. The ratio $A_T / \bar{A}$ may be related to the ratio of turbulent to laminar flame speed (s_T / s_{L0}), following Damköhler [15]. This implies a relation to the turbulent flame speed closure (TFC) approach of Zimont and Lipatnikov[16], where the turbulent flame speed is calculated with an algebraic approach. The closure is directly applied to the flame-wrinkling ratio $A_T / \bar{A}$, leading to

$$\bar{\dot{w}}_c = \rho_u s_{L0} \frac{A_T}{\bar{A}} |\nabla \tilde{c}|$$

The flame-wrinkling ratio is modelled as

$$\frac{A_T}{\bar{A}} \sim \frac{s_T}{s_{L0}} = 1 + \frac{0.46}{e^{(Le-1)}} \mathrm{Re}_t^{0.25} \left(\frac{u'}{s_{L0}} \right)^{0.3} \left(\frac{p}{p_0} \right)^{0.2}$$

where p / p_0 is the ratio of the operating pressure to the atmospheric pressure, Le is the Lewis number.

2.4 Importance of Lewis Number in Premixed Combustion

For lean methane flames the thermal diffusivity is nearly equal to the molecular diffusivity of the fuel, leading to a $Le \sim 1$. For larger hydrocarbon fuels, it is typically >1.

Industrial Combustion
Journal of the International Flame Research Foundation
Article number 201618, June 2020
ISSN 2075-3071

Its effect is directly connected to the molecular heat and mass transport into and away from the reaction occurring flame zone. A decrease in flame velocity occurs for $Le > 1$, because thermal diffusivity exceeds molecular diffusivity. Therefore, the rate of heat losses from the reaction zone exceeds the rate at which the reactant is transported into the reaction zone.

Our earlier studies [9, 17] have shown that this phenomenon of local flamelet quenching by turbulent eddies must substantially depend on the Lewis number. For higher Lewis number fuel-air mixtures ($Le > 1$), maximum growth rate and the wave number at the maximum growth rate are much smaller than for near-unity Le fuel-air mixtures. This is due to the effects of large Le that enhance the diffusive thermal effects to restrain the flame instability. Smaller maximum growth rate and smaller wave number at the maximum growth rate cause the smaller increase in total flame area, resulting in smaller increase in turbulence flame propagation, having for example application in lean burning automobile engines.

In the algebraic combustion model, the exponential dependency $1/e^{(Le-1)}$ is consistent with the leading point model by Lipatnikov and Chomiak[18]. The effect of the preferential diffusion (PD) is observed for the cases when diffusivity difference of the fuel from the oxidizer is distinct and the concentration of a larger diffusivity species of the fuel or oxidizer is deficient. Characteristically, PD is evaluated using for example the local burning velocity and the local equivalence ratio. These two quantities are evaluated at the leading edge of the flame with positive curvature on the downstream of the flame, i.e., facing towards the unburned premixed mixture. These two quantities are expected to qualify the leading flamelet of highest flame propagation[18, 19]. Its significance is realizable in, lean and rich light and heavy fuel-mixtures, predominantly at high turbulence and for low laminar flame speeds. Halter et al.[20]have experimentally evaluated the characteristics of mixed fuels, with shorter flames at higher pressures. Recently, Jiang,Y. et al.[21] have shown that turbulent flame speed is strong function of equivalence ratio, and at low fuel to air mixture, turbulent velocity is more predominant.

2.5 Dynamics of Swirl Flames

The simplest way of stabilisation of flame is behind a sudden expansion like a backward-facing step. The flow strongly decelerates and forms an outer recirculation zone (ORZ). The recirculation zone stabilises the flame through mixing of burned gases with the incoming fresh mixture. On inducing swirl for such a flow makes the flame much compact, or rather sandwiched between low-velocity zones. The swirling flow forms a central recirculation zone (CRZ) that acts as a flame holder in the centre of the flow. Fig. 1 shows the sketch of the flow characteristics of a swirling flow. A study by Zhou et al.[22]predicts that the change of equivalence ratio has substantial effect on highly swirl reacting flows.

Industrial Combustion
Journal of the International Flame Research Foundation
Article number 201618, June 2020
ISSN 2075-3071

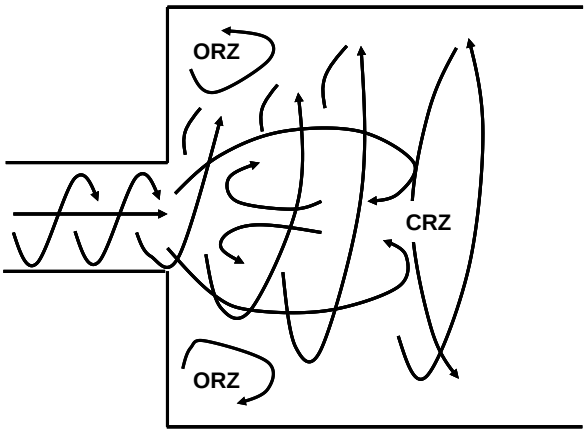

Figure 1: *Schematic of a swirl flow depicting CRZ and ORZ*

Due to the excellent flame holding, mixing, burnout and emission characteristics, swirling flames are exclusively used in gas turbine combustors. The reliability of swirl burners is determined by its capability to prevent flashback into the mixing zone. Flame flashback is an intrinsic behaviour of premixed systems as the flame may stabilize where fuel and oxidizer mix, upstream of the combustion chamber. Despite of the well-developed theories on flashback, for example [23, 24], the type of flashback occurring in lean-premixed GT combustors is not clearly defined. Understanding flame propagation and stabilization in the mixing zone of these configurations is essential either to avoid flashback or to set the flashback limits of a particular burner. Flashback can occur due to Baroclinic push. This phenomenon occurs due to coupling of the density gradient across the flame (occurring due to difference in unburned and burned gas velocities) and the radial mean pressure gradient in the unburnt swirling gas ahead of the flame, results in generation of azimuthal vorticity [24, 25] counter acting against the axial jet in the mixing tube. Despite of the turbulent flame speed being lower than the axial jet, as the azimuthal vorticity enhances the flame propagation by retarding the axial jet. This 'push' is quantified in the swirling flows discussed later below.

3. Simulated Geometries and Experimental Details

3.1 Sudden Expansion Dump Combustor (F1-Configuration)

Measurements on this configuration were performed on a cylindrical sudden expansion dump combustor at *Paul Scherrer Institute* (PSI)[5]. Because of underlying advantages due to high-efficacy and low emissions, energy conversion of gaseous fuels, turbulent premixed combustion rapidly spread its wings into technical applications, finds its place especially in stationary gas turbines (GTs). These studies are of significant relevance owning to (preheated) high-pressure and high turbulence levels, with operations close to stationary GT inlet conditions. This test rig designed for a maximum thermal power of 400 kW can have a maximum operating pressure of 30 bar, airflow rate of 750 Nm^3/h, air can be preheated up to 823 K with an electrical heater and can withstand exhaust gas temperatures up to 1850 K.

Industrial Combustion
Journal of the International Flame Research Foundation
Article number 201618, June 2020
ISSN 2075-3071

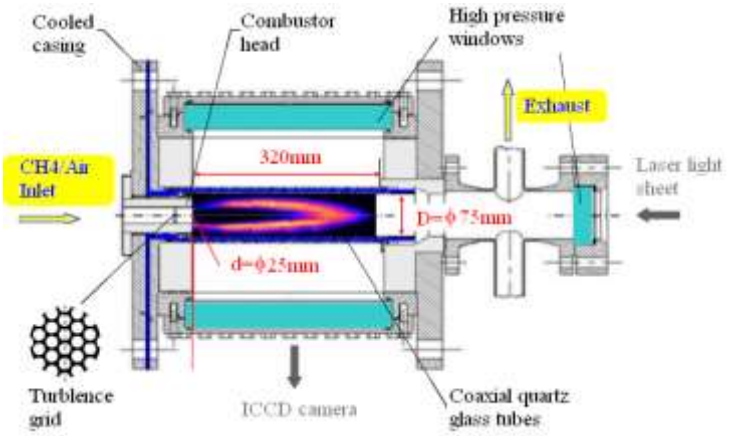

***Figure 2**: Experimental high-pressure combustion chamber of Griebel et al. [5]*

The test rig marked with all the important accessories is shown in Fig. 2 and flame configuration is here after referred as F-1. It consists of two coaxial quartz glass tubes (inner quartz glass tube diameter *D* = 75 mm) which are convectively air-cooled and the combustor inlet diameter *d* is 25 mm. The flame is stabilized aerodynamically via the outer recirculation of hot flue gases, induced by the combustor geometry with sudden expansion (Fig. 3). The three large high-pressure windows provide the optical access required for non-intrusive laser diagnostics. Inlet turbulence was generated with a turbulence grid having hexagonal pitch with a hole diameter of 3 mm, placed at 30 mm upstream of the sudden expansion. In this configuration, only the cold flow velocity field was measured with the help of 2D Particle Image Velocimetry (PIV). The mean axial velocity and turbulent kinetic energy in the centre plane along the combustor axis after the sudden expansion are available for the numerical validation.

The turbulent flame regime analysis (Fig. 4) show that with increase of pressure, the flame conditions move into the thickened reaction zone ($Ka > 1$), with the reduction of the Kolmogorov scale (which is smaller than flame thickness at high pressures).

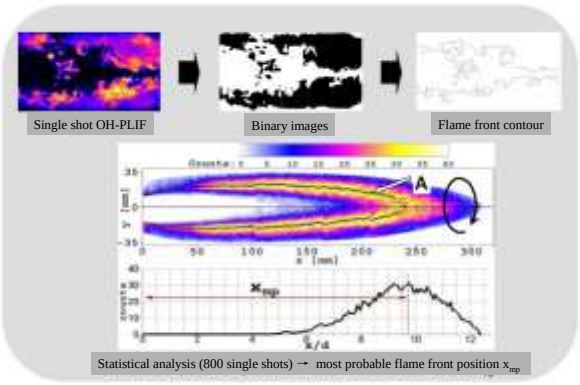

***Figure 3:** Flame front detection method and most probable flame front position estimation[5]..*

Industrial Combustion
Journal of the International Flame Research Foundation
Article number 201618, June 2020
ISSN 2075-3071

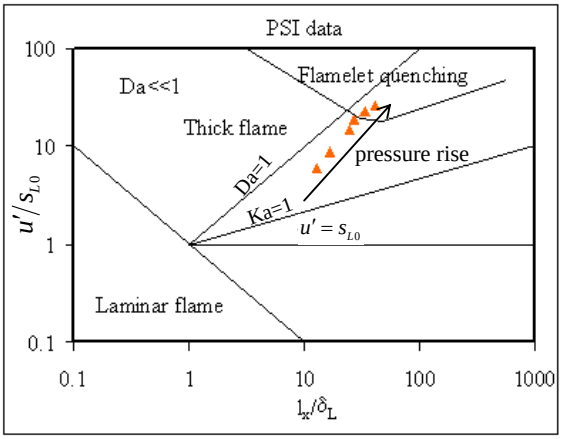

***Figure 4**: High-pressure flames from PSI [5]. plotted into the Borghi diagram with turbulence quantities measured at the sudden expansion region.*

The general flow characteristics of F-1 configuration are grid-generated turbulence is dominant in the core flow region and shear-generated turbulence in the post-region (downstream side) of the flame. Table: 1 shows the simulated cold flow cases for F1 configuration and Table 2 shows the reacting cases. This data enables to extend the combustion model to LES.

3.2 Swirl Flow Burner Systems

As mentioned in the introduction, one of the goals of this study is to test the AFSW turbulent premixed combustion model that may be usable for varied fuels at high pressures. This is tested with two different configurations of swirl flow gas turbine burners without and with mixing tube. The purpose of the mixing tube is to ensure better mixing of fuel and air before the combustion zone to reduce the NO_X emission to ultra-low levels. These two configurations are F-2(Fig.5).

***Figure 5:** Conical gas turbine burner, F-2 is a conical burner with mixing tube*

With the F-2 configuration, both fuel and high-pressure influences and behaviour of the novel reaction closure at gas turbine conditions are studied in RANS context. For this configuration detailed experimental data is not available. Nevertheless, this configuration is useful for the numerical study, where the importance of the fuel influence in the reaction closure is demonstrated by artificially varying the Lewis number of the fuel air mixture for a liquid fuel (assuming the properties of n-heptane) at an operating pressure of 14 bar. The flame stabilisation mechanism is explained with relevant theoretical justification. We studied the progression of the flame stability of this burner for three adiabatic flame temperatures 1650 K, 1700 K, and 1800 K. More details about this burner and its behaviour are furnished in the subsequent sections.

Industrial Combustion
Journal of the International Flame Research Foundation
Article number 201618, June 2020
ISSN 2075-3071

3.3 Simulation Matrix

Cold flow simulations are performed for two different configurations of F-1, the details of which are given in Table 1. Both cold and reacting flows are simulated in the RANS and LES contexts for F-1 configuration, to ascertain the advantages and limitations of each one through relative comparison of flame data. In the LES cases, three turbulence sgs closures – the classic Smagorinsky, dynamic Smagorinsky, and one-equation kinetic energy transport equation – are used.
Table 2 gives overview of reacting studies performed for F-1 a sudden expansion dump configuration from [5]and the conical burner configuration as F-2. The AFSW model has been verified in both RANS and LES contexts. Benim et al.[26] in LES comparative studies using two different commercial codes show very good quantitative agreement for shear flows and stabilization of flame with measurements, a lean methane/air mixture at 8 bar. In our study, we investigate the flame stability for a range of pressures and equivalence ratios (Tables 1&2).

Table 1: Test matrix of the cold flow simulations, depicted are the 3D outline of the dump combustor (F-1)

Name	Geometry	P(bar)	RANS	LES		
				SM	DS	K_{SGS}
F-1		1	✓	✓	✓	✓
		1, 10	✓	✓	✓	✓

Table 2: Test matrix of the combusting flow simulations, shown are the 2D cross-sectional views along the axis of the respective geometries

Name	Geometry	Le	P(bar)	RANS	LES	Fuel profile
				AFSW	AFSW	
F1		1.0	1,5,10	✓	✓	Fully premix
F2		1.0	1, 16, 32	✓	--	Fully premix
		1.0,1.3, 1.8, 2.3	14	✓	--	Rich core & Lean outer

The applicability of the AFSW model as subgrid scale reaction closure is tested in LES approach F-1. The employed turbulence models and the numerical schemes along with the grid details are presented in Table 3.

Table 3: *The employed turbulence models in RANS and LES, numerical schemes, and grid details (CDS-Central Difference Scheme, TKE-Turbulent Kinetic Energy, TDR-Turbulent Dissipation Rate).*

	for RANS	for LES
Turbulence models	Standard $k-\varepsilon$ model	The Smagorinsky The dyn. Smagorinsky The dynamic k_{SGS}
Pressure	II-order	II-order

Industrial Combustion
Journal of the International Flame Research Foundation
Article number 201618, June 2020
ISSN 2075-3071

Momentum	II-order upwind	II-order CDS
Pressure-Velocity Coupling	SIMPLE	SIMPLE
TKE, TDR	II-order upwind	-
Progress Variable	II-order upwind	II-order CDS
Temporal Discretisation	-	II-order
k_{SGS}	-	II-order CDS
Grid spacing	≈ 1 mm (3D-RANS) ≈ 0.25mm (2D-RANS)	≈ 1 mm (fine) ≈ 2 mm (coarse)
Cell count	≈ 6 million (3D-RANS) ≈ 45,000 (2D-RANS)	≈ 1.1 million (fine) ≈ 0.4 million (coarse)
Smagorinsky's model Const.(C_s)	-	0.1 (actual solution) 0.05 (for analysis)

4. Outcome of Numerical Simulations

4.1 Cold Flow RANS Simulations (F-1 Configuration)

Non-reacting simulations are performed using RANS $k-\varepsilon$ (model) approach on a three dimensional domain to study the influence of the turbulence grid located at 30 mm upstream of the sudden expansion (Fig. 2). The operating conditions and the geometric Reynolds number (Re) of the non-reacting and reacting cases are given in Table 4. The nomenclature: C_COLD represents the cold case, C_COMB represents the combusting case and the following number represents the operating pressure.

The whole computational field is meshed unstructured with nearly six million tetrahedral cells in Table 3, after reaching grid independency test. The dimensions of the holes, pitch, and placement of the turbulence grid replicate the experimental setup shown in Fig. 2. Typical flow characteristics of the simulated geometry are numbered in Fig. 6, where '1' is the high velocity core flow region with grid-generated turbulence, '2' is the recirculation region formed due to sudden expansion, in between these two, is '3', the region of shear generated turbulence, which extends to the downstream region.

Table 4: *Operating conditions of the selected cases (units in m/s, K, and bar)*

Case	U_{in}	T_{in}	p	Re	RANS	LES	T_f/T_{in}
	m/s	K	bar	-	-	-	K
C_COLD1	45	300	1	81,000	YES	YES	300
C_COLD5	45	673	5	405,000	YES	NO	300
C_COLD10	45	673	10	810,000	YES	NO	300
C_COMB1	45	673	1	16,000	YES	YES	1750
C_COMB5	45	673	5	80,000	YES	YES	1790
C_COMB10	45	673	10	160,000	YES	YES	1795

Industrial Combustion
Journal of the International Flame Research Foundation
Article number 201618, June 2020
ISSN 2075-3071

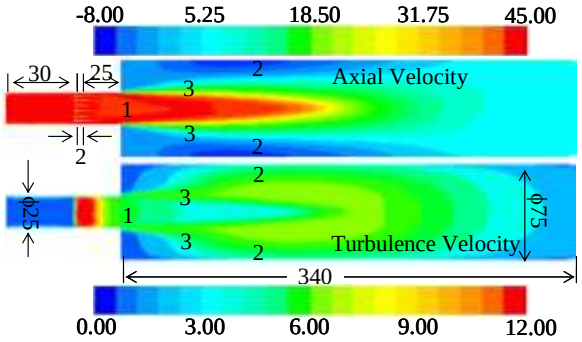

Figure 6: *Predicted axial (top) and turbulent (bottom) velocities by the $k-\varepsilon$ model, regions of the different flow characteristics are marked with numbers (dimensions in mm).*

The radial profiles from 5 mm downstream of the turbulence grid (x = – 25 mm) up to the sudden expansion (x = 0 mm) indicates the penetration of the jets into the combustor (sudden expansion), see Fig. 7.

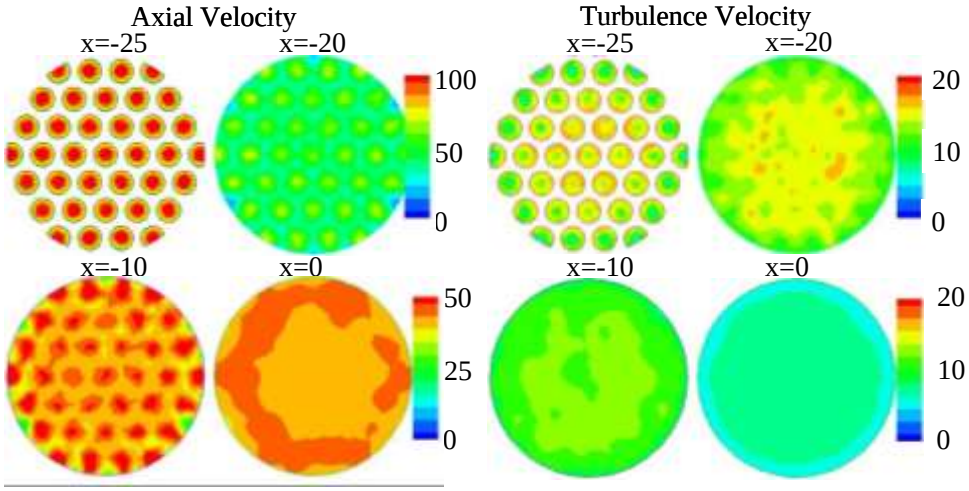

Figure: 7.*Predicted axial and turbulent velocities by the $k-\varepsilon$ model, at different levels upstream of the sudden expansion (x = 0 mm corresponds to the sudden expansion location and -25 mm to the location of the turbulence grid).*

The contours in Fig. 6 are graphed in Fig. 8 for normalized mean velocity and axial turbulent kinetic energy (TKE) profiles along the axis of the combustor. This shows, the jet break-up length is over predicted twice the size of inlet diameter. Though the TKE peak is predicted reasonably, its width in the axial direction is very narrow (Fig. 8, right). To reduce the computational burden, 2D axis-symmetric simulations are performed for the domain behind the turbulence grid by imposing constant inlet velocity and turbulence levels for varied pressures. These subordinate results are close to the 3D simulation, except in the region of x/d < 2.5 where the TKE in the 3D case is higher due to the penetration of the mentioned individual jets produced by the turbulence grid. The main TKE peak is predicted very similar to that in the three dimensional case and jet break-up length is slightly extended downstream by 0.2 d. As assumed, the significance of the pressure at least up to 10 bar in 2D RANS non-reacting flows is less significant (Fig. 8).

Industrial Combustion
Journal of the International Flame Research Foundation
Article number 201618, June 2020
ISSN 2075-3071

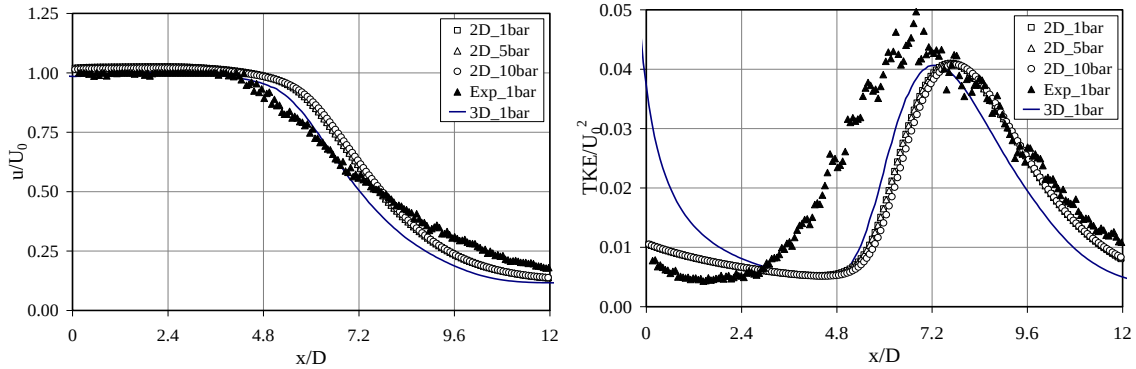

***Figure 8**. Comparison of axial velocity (top) and TKE (bottom) of 2D and 3D cases with that of experiments along the axis of the combustor. It includes high-pressure cases in 2D domain.*

Fig. 9 shows he radial profiles at three axial junctions of x/d = 1, 5 and 11. As noted above, the axial velocity predictions in both 2D and 3D simulations at the first two junctions closely follow the experiments but the TKE mismatches considerably, especially in 3-D. Our effort to tune the $k-\varepsilon$ turbulence model constants $c_{\varepsilon 1}$ and c_{μ}, yielded very little success.
Following these reprehensible RANS results, we present more satisfactory results of these complex characteristics of dynamic flows.

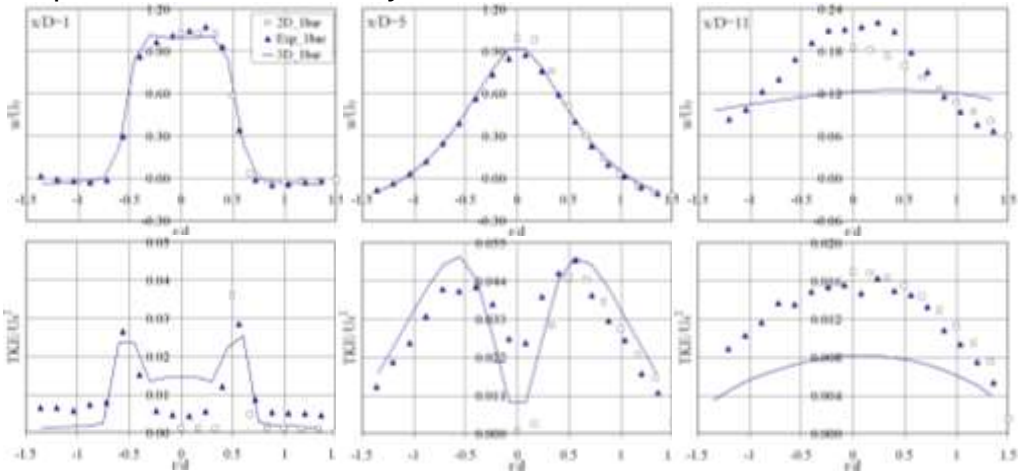

***Figure 9.** Comparisons of axial velocity and TKE of 2D and 3D cases with experiments at three different axial locations in the combustor*

4.2 Non-reacting flows: LES (F-1 Configuration)

Cold flow simulations using the Smagorinsky, dynamic Smagorinsky and one-equation k_{sgs} turbulence closures. The flow characteristics, the employed numerical schemes and the simulated cases are given in Tables 3 and 4. Atmospheric cold flow simulations are performed for the three turbulence closures for varied inflow conditions and grid types. As the inlet turbulence grid is situated 30 mm upstream of the sudden expansion, two test simulations are performed one with constant inlet velocity of 45 m/s and the other for a *specified* inlet profile, retrieved from RANS on a domain extending 82 mm downstream of the sudden expansion.

Industrial Combustion
Journal of the International Flame Research Foundation
Article number 201618, June 2020
ISSN 2075-3071

The computational domain is meshed in two modes, one resolved only near the wall and uniform elsewhere, and the other resolved in the shear layer and near walls. For the former grid, two grid resolutions (fine and coarse) are used to estimate the resolved energy using the LES_IQ analysis[27]. We show that fine grid simulations correspond to the actual results.

In Fig. 10a, b and c show the axial profiles of mean axial velocity and the resolved turbulent kinetic energy (TKE) of all the cases obtained with the fine grid. Irrespective of the specified inlet boundary conditions and the turbulence model used, the experimental behaviour cannot be reproducible between x/D = 0 and x/D = 3. However, the inlet condition has very little influence in predicting the jet break-up length and the TKE peak with the classical Smagorinsky model. In other words, the break-up is dependent mainly on the shear-generated turbulence between the strong axial jet and the recirculation zone (Fig. 11). An interesting finding is that for the dynamic models, the inlet profile has strong influence on the velocity field predictions and minimal impact on resolving the shear layer.

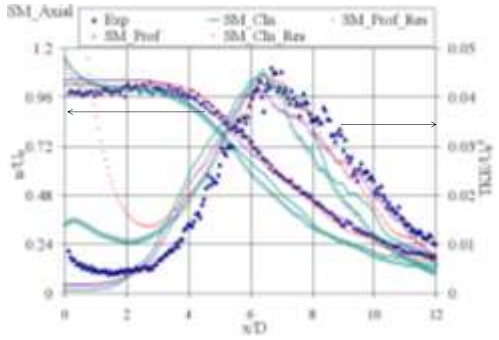

Figure 10a: *Axial profiles of the Smagorinsky (SM) closure on fine grid for varied inlet conditions, CIn – represents constant inlet profile with specified perturbations at the inlet on uniform grid, Res - with grid resolved in shear layer, prof – specified inlet velocity profile as shown in Fig. 8.2 (x = 0 mm), Exp – Experiments.*

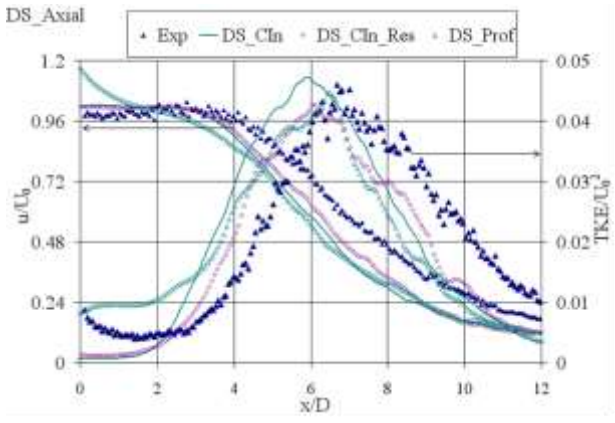

Figure 10b: *Axial profiles of the dynamic Smagorinsky (DS) closure on fine grid for varied inlet conditions, CIn – represents constant inlet profile with specified perturbations at the inlet on uniform grid, Res - with grid resolved in shear layer, prof – specified inlet velocity profile as shown in Fig. 8.2 (x = 0mm), Exp – Experiments.*

Industrial Combustion
Journal of the International Flame Research Foundation
Article number 201618, June 2020
ISSN 2075-3071

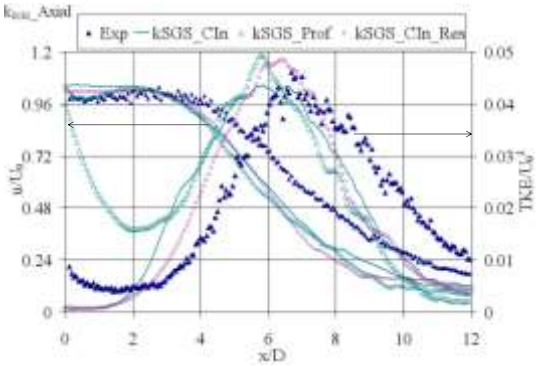

Figure 10c: *Axial profiles of the dynamic k_{sgs} closure on fine grid for varied inlet conditions, CIn – represents constant inlet profile with specified perturbations at the inlet on uniform grid, Res - with grid resolved in shear layer, prof – specified inlet velocity profile as shown in Fig. 8.2 (x = 0mm), Exp – Experiments.*

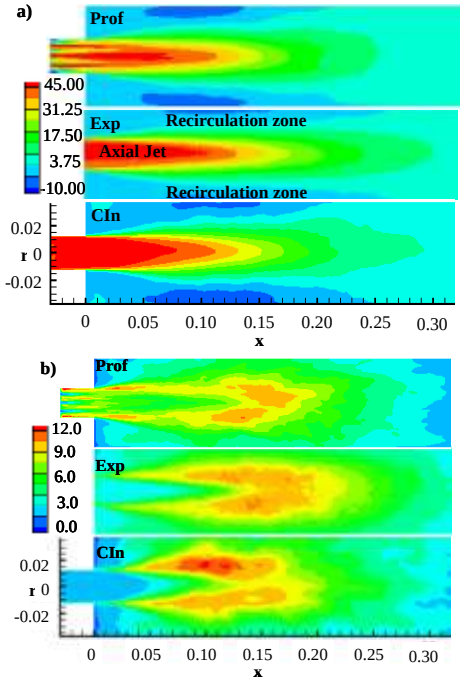

Figure 11. *Contours of a) mean axial velocity and b) axial RMS velocity obtained on an uniform grid with inlet jets (Prof) and with constant inlet velocity (CIn) in comparison with that of experimental findings Exp).*

In Fig. 12, the results obtained from the Smagorinsky model on coarse and fine grids are compared with the experiments. The convergence of the cases is dependent on the grid and SGS model employed (Pope et al 2012). All the models predict a longer jet on the coarse grid in comparison to the fine grid with over-prediction of TKE. This is attributed to lower resolution that reduces the dissipation rate. Another interpretation is that the coarse resolution corresponds to a flow at an effectively lower Reynolds number. Therefore, the transition to shear induced turbulence is delayed, while a higher dimensionless kinetic energy is predicted; the estimated Re_t along with viscosity is shown in Fig. 13a. This is in accordance with DNS observations [28]. The viscosity on the coarse grid is 2-3 times higher than that of the fine grid. The time-averaged model coefficients of the three turbulence models on the fine grid are shown in Fig. 13b along

Industrial Combustion
Journal of the International Flame Research Foundation
Article number 201618, June 2020
ISSN 2075-3071

with the strain rate magnitude, which is used to estimate the subgrid turbulent intensity and length scale.

The LES accuracy of the three models is estimated with the method proposed (using Eq. 5.3) by Celik et al. [27] is shown in Fig. 13c. Between x/d = 2 and 9 all three models result in the same accuracy about 60 %. Beyond x/d = 9 (downstream of the TKE peak) the classic Smagorinsky model yielded better than the dynamic models. Thus, it is not always valid to assume that the dynamic Smagorinsky model outperforms the Smagorinsky model. This point was illustrated by Meneveau [29] for rapidly strained flows. Moreover, the implementation of the dynamic model differs from case to case and from code to code in the way the dynamic coefficient is limited and averaged. It is usually averaged in the direction that is considered to exhibit homogeneity in turbulence. In more complex cases, as has been dealt here; there is no obvious homogeneous direction. The strong variations of the dynamic models with shear layer resolution and with inlet profile (Fig. 13a, b, & c) is attributed to its implementation.

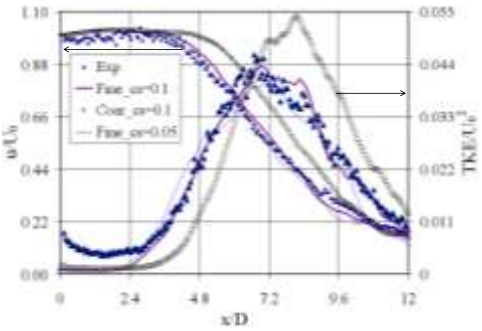

Figure 12: *Profiles of mean axial velocity and TKE along the combustor axis predicted by the Smagorinsky closure on coarse and fine grids for the case C_COLD1. Distinguished differences between the coarse and fine grids are visible, but very minor differences between the cases simulated with* C_s *= 0.1 and* C_s *= 0.05 on the fine grid level.*

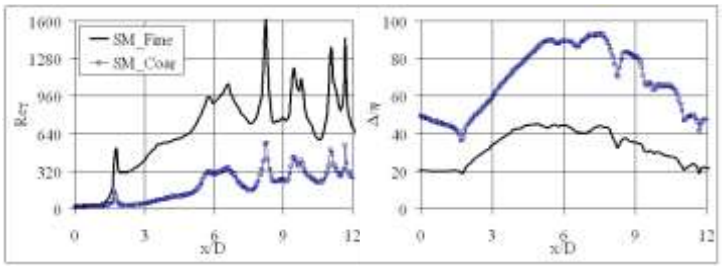

Figure 13a: *Estimated* Re_t *on coarse and fine grid (left) along with the time averaged viscosity (right) for the Smagorinsky model.*

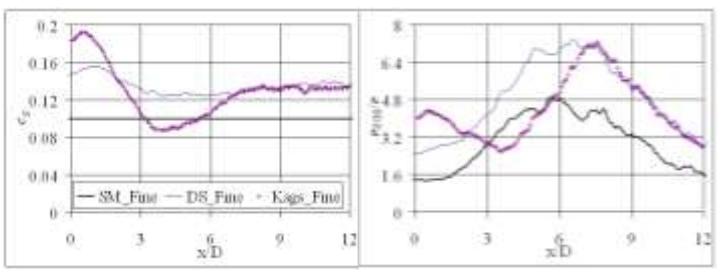

Figure 13b: *Time averaged turbulence model constant (left) and strain rate magnitude (right) of the three models.*

Industrial Combustion
Journal of the International Flame Research Foundation
Article number 201618, June 2020
ISSN 2075-3071

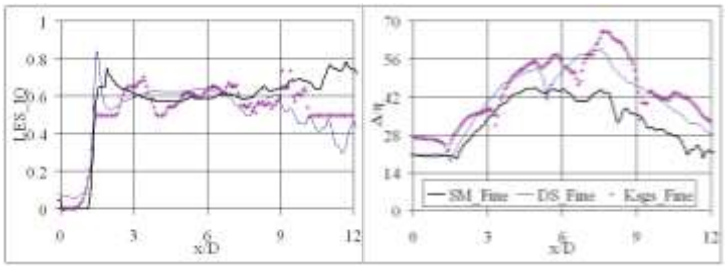

Figure 13c: *LES_IQ for three turbulence models (left) and the ratio of the grid size to the effective Kolmogorov scales (right), both giving indication of the good LES resolution on the fine grid level.*

The individual error contributions (estimated with Eqs. 5.7, 5.8 and 5.9) of the turbulence model and discretization scheme towards the total energy is estimated with Klein's approach [30]. Computed mean axial velocity and turbulent kinetic energy (TKE) on the fine grid are in close proximity with measurements (Fig. 12). The figure also shows the change of the Smagorinsky constant C_s from 0.1 to 0.05 there is no considerable difference in the quantification of mean velocity and TKE. In particular, for the combination coarse grid with C_s=0.1, the peak TKE is over-predicted by as much as 30%. In all three cases the Klein's approach is used to estimate the amount of energy dissipated via discretization and from the usage of the turbulence closure. Fig. 14 shows the model and numerical contributions, and the total contribution are having opposite signs, so summed up they contribute less to total error contribution.

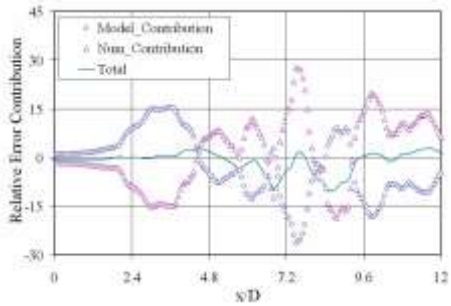

Figure 14.*Separation of numerical and model error contributions (estimated with Eq.5.7, 5.8 and 5.9) plotted along the axis of the combustor obtained with the Klein's approach*

4.3 Reacting Flow LES (F1- Configuration)

We present combustion LES for each of these three sub-grid turbulence closures in combination with the AFSW reaction model (Eq. 7.9). This section is apportioned into three sections; Comparison of cold and combusting flow cases, Interaction of - turbulence and reaction closures and LES of high-pressure flames.

4.3.1 Comparison of cold and combusting flow cases

The cold (C_COLD1) simulations performed with the Smagorinsky model are compared and analysed with the three high-pressure reacting cases (C_COMB1, C_COMB5 and C_COMB10) simulated with the AFSW model, in combination with the three sgs models. This study specifically assesses the changes because of

Industrial Combustion
Journal of the International Flame Research Foundation
Article number 201618, June 2020
ISSN 2075-3071

combustion heat release. Similar to typical gas turbine conditions the reaction mixtures are preheated to 673 K. This decreases the Reynolds number at the inlet to about 16,000 which is 20% of that in the cold flow. In Figure 15a, the averaged axial velocity and the turbulent kinetic energy profiles are shown along the burner axis. It can be noticed from Fig. 15a that the transition to large-scale turbulence takes place more downstream in the combustion case (x/D = 6, Fig. 15a) compared to the non-reacting situation (x/D = 3, Fig. 15a).
The evaluated LES index of quality is shown along the axis in Fig. 15b for the cold and the combustion case. The higher value in combusting flow is due to the reduction of the Reynolds number, reaching a value of around 0.8, compared to 0.6 for the cold flow. This is a straightforward indication of well-resolved LES for the combustion flow. This can be confirmed from estimated Kolmogorov scales, □ that reducing the ratio between grid size h and □ from 20–40 in the cold case to 4–8 for the combustion case (Fig. 15b). The finest (Kolmogorov) scale □ is calibrated based on the effective viscosity, which is estimated, following[27], as sum of molecular, turbulent, and numerical viscosities ($\nu_{mol} + \nu_t + \nu_{num}$). Similar results have been found also for the dynamic models not presented here.

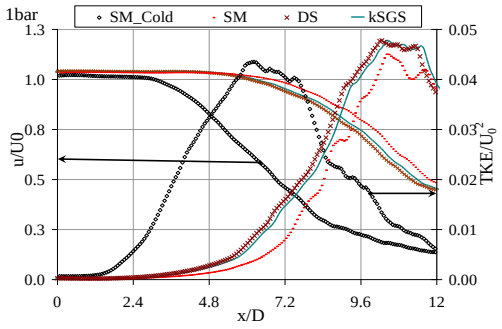

Figure 15a: *Profiles of mean axial velocity and TKE along the x-axis predicted with the three closures in comparison with the cold flow predictions.*

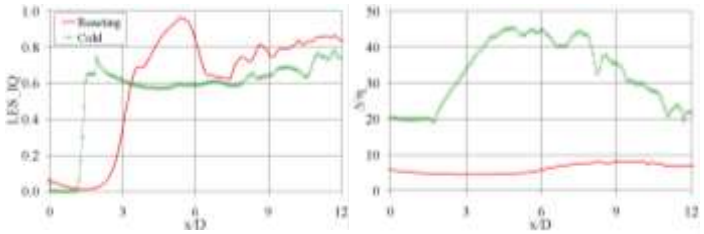

Figure 15b: *LES IQ obtained from two grid levels showing the amount of resolved kinetic energy (left) and the grid size w.r.t. Kolmogorov scale (right) in non-reacting (C_COLD1) and reacting cases (C_COMB1).(Smagorinsky model, 1 bar).*

4.3.2 Interaction between -turbulence and reaction closures

In the first instance, turbulent lean premixed methane flames are simulated for all the three turbulence closures, along with the algebraic flame-wrinkling reaction model at 1 bar (Fig. 15c). The time-averaged gradient of the reaction progress variable as indicator of the flame position is compared with experimental data (Fig. 15c).
The calculations with LES result in the flame length which is remarkable close to the experimental situation. This is in contrast to the RANS calculations (as shown in Fig. 8), where the flame was over predicted by 30%. A more detailed comparison between experiment and LES calculations shows, that the reaction closure in combination with

Industrial Combustion
Journal of the International Flame Research Foundation
Article number 201618, June 2020
ISSN 2075-3071

the two dynamic models follows the experimental data more closely whereas with the standard Smagorinsky model the flame position is shifted downstream by about 10 %. This is opposite to the cold flow simulation in which the Smagorinsky model was found in better agreement with the experimental data in terms of mean axial velocity and TKE.

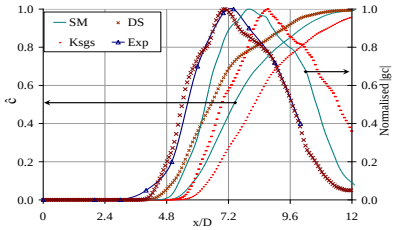

Figure 15c: *Profiles of progress variable along the combustor axis predicted with the AFSW model in combination with three closures. Also plotted is the progress variable gradient of the three combinations along with the experimental data for 1bar case.*

4.3.3 LES of high-pressure flames

The increase in pressure is made in two steps, from 1 to 5 and to 10 bar, for constant inlet flow conditions for lean equivalence ratio of 0.5. In Figure 16a, computed instantaneous sample flames in the plane of the axis are shown in comparison with instantaneous OH-PLIF images in the same plane (field of view is different). Although the interpretation of such OH-PLIF images with respect to the reaction zone is not appropriate (the gradient in the inner part between zero and maximum OH may be assumed in first order to mark the instantaneous reaction zone), the comparison between the instantaneous LES planes and the experimental images is remarkable. From 1 to 5 bar, the flame becomes highly wrinkled and distorted for both, experiment by Griebel et al. [3]and present LES study. This is a direct indication of increased flame surface area, and thus increased reaction rate. This finding fits to the expected decrease of the smaller turbulence scales (the Kolmogorov length scales with $\eta \infty p^{-3/4}$). Similar assessments of the pressure effects on the dynamic range of turbulence structures and the flame front wrinkling were made by Soika et al[31].

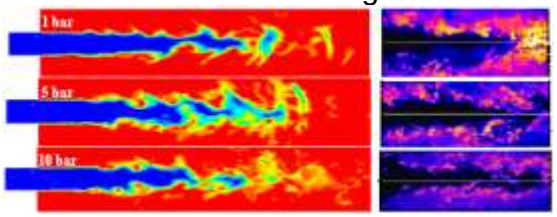

Figure 16a: *Instantaneous progress variable contours, for 1, 5 and 10 bar, using the Smagorinsky model (left), compared with instantaneous OH-PLIF images (right). (Inflow velocity is hold constant U = 45 m/s, methane/air ϕ = 0.5, preheated T_0 = 673 K).*

Interestingly, the visual influence of pressure on flame wrinkling is less pronounced for the step between 5 and 10 bar, as compared to that up to 5 bar. This difference has also been observed experimentally [32] and[33] citing [4]. The two possible reasons for this behaviour are: 1)The changing pressure dependency of the laminar flame speed $s_{L0} \infty p^{x}$, where the exponent x decreases from 0.58 to 0.45 with pressure, following laminar flame data,
2) The relative pressure ratio is 5 for 1 to 5bar and 2 for 5 to 10bar.

Industrial Combustion
Journal of the International Flame Research Foundation
Article number 201618, June 2020
ISSN 2075-3071

As noted above, the reaction sub-closure (Eq. 7.9) for the flame-wrinkling ratio has been found to be capable of yielding high-pressure effects on the reaction rate due to the presence of an explicit non-dimensionalized pressure term p/p_0. Experimental studies by Lachaux[4]has given a similar dependency on pressure-turbulence relation given by up to 9bar, support our findings. Experiments yielded a constant mean turbulent flame brush thickness and only very small effects of pressure on the distribution of the time averaged statistical OH contour from 1 to 10 bar [5] (note, that not the absolute OH concentration has been compared, which varies by several reasons with pressure, but the statistical instantaneous flame contour position, for which the individual OH images have been binarized on a low OH-level). The employed reaction closure predicted trends quite similar to these observations. Simulations have shown a marginal increase of flame brush with pressure in the axial direction (Fig. 16b and c), where in RANS approach the reaction model predicted very thin flame brush.

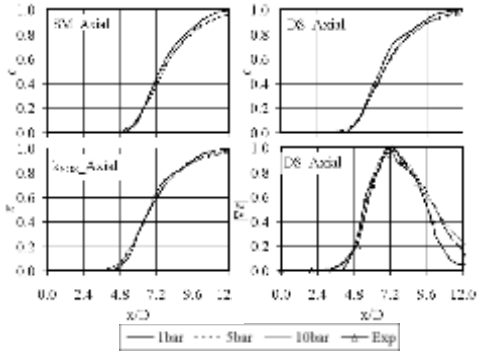

Figure 16b: *Behaviour of the reaction model with all the three closures for pressure variation, from 1 to 10 bar. Shown are axial profiles of time-averaged progress variable, for the dynamic Smagorinsky model also the progress variable gradient.*

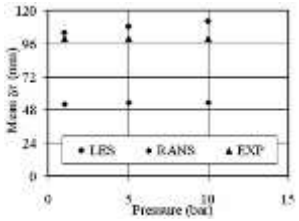

Figure 16c: *Time averaged flame brush thickness along the axis plotted for pressure variation, shown for LES, experiment, and RANS.*

The increase of reaction rate with pressure is apparent from instantaneous pictures (Fig. 16a). The increase of the time-averaged flame wrinkling and mean reaction rate with pressure can be seen in Fig. 17. Overall, the reaction closure in combination with the three models has yielded excellent results. The reaction model in combination with the dynamic Smagorinsky model has been in good agreement with the experimental OH-PLIF data than with the other two models. It is worth-noting that, at high pressure due to enhanced turbulence scale spectrum, the modelling contribution of handling the scales increases. This effect can be observed from Fig. 17 (bottom), which shows an increase in -viscosity with pressure. There is an increase in the flame area $A_T/\bar{A}$ with pressure, i.e. increased reaction rate. At 1 bar, the maximum time-averaged field quantity $A_T/\bar{A}$ in the axial direction is 1.2, whereas 1.8 and 2.2 are realized at 5 and 10 bar respectively.

Industrial Combustion
Journal of the International Flame Research Foundation
Article number 201618, June 2020
ISSN 2075-3071

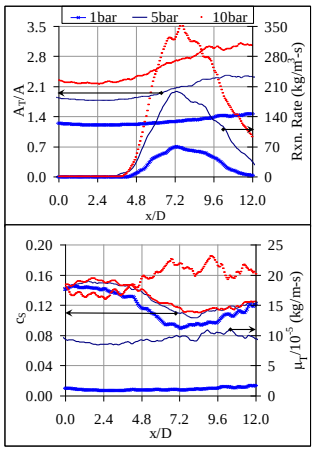

Figure 17: *Time averaged flame wrinkling ratio, reaction rate (top), the dynamic Smagorinsky constant and viscosity(bottom) for the three reacting cases.*

To summarize, in reacting flows, The LES_IQ for cold and combusting flows were, respectively, 50-60% and 80%. The numerical and model contributions are estimated using the Klein's approach. The reaction closure was successfully validated against experimentally measured mean flame position and flame brush thickness. Also, for increased pressures, the combustion LES results were in excellent agreement w.r.t these two quantities. Increase of flame wrinkling was clearly noticeable in the computed instantaneous flames. RANS studies yielded reasonable mean flame length, while under predicting the axial turbulent flame brush width by as much as 50%.

4.4 Reacting Flow Simulations of Swirler Burner (F2-Configuration)

We studied in RANS the swirl flow gas turbine burner systems, a conical swirl burner (F2) for varied pressures and Lewis numbers in RANS for two different fuel profiles. The performance of F-2 configuration is studied for variation of pressure, flame temperature and Lewis number in RANS context. The reacting flow RANS is performed utilising the AFSW reaction closure. The temperature and pressure variations are performed for fully premixed Methane-Air mixture. Whereas the Le variation is performed on the same configuration with a fuel profile of Rich core and Lean outer representing liquid fuel injection from the centre line of the burner. In this study pre-vapourised liquid fuel (n-heptane) is considered for Le of 1.3, 1.8 and 2.6as a function of mixture fraction.

The numerical outcome obtained on the conical swirl (F-2) burner[34], aWe performed simulations of lean pre-vapourised premixed (LPP) diesel-air mixtures to signify the importance of the Lewis number. As diesel fuel is made of several constituents, it is rather hard to derive correct Le value; moreover, it further lessens the accuracy for varied equivalence ratios. On the other hand, the other important physico-chemical property, the laminar flame speed, of diesel vapour mixtures is taken from[35]. The local concentration of fuel-air mixture in the LPP case is accounted by solving an extra transport equation for the mixture fraction.

The schematic of the burner configuration is given in Fig. 18. Liquid fuel is injected at the cone which mixes with the air entering through the air slots of the swirler cone. The gaseous fuel is injected through the holes distributed along the inlet slots. Fuel and air are homogenously premixed in the case of fuel gas operation. In the liquid fuel case, the fuel is injected along the centre line of the burner. In the current study for simplicity

Industrial Combustion
Journal of the International Flame Research Foundation
Article number 201618, June 2020
ISSN 2075-3071

pre-vapourized fuel is considered as the focus is on the importance of fuel profiles for variations of fuel types

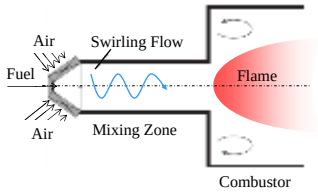

Figure 18: *Schematic of the conical burner showing the swirler, mixing zone and combustor.*

4.4.1 Influence of Flame Temperature and Pressure on Flame Stability

For this configuration (F-2), experimental data is not available for the comparative purpose. The model predictions are presented firstly for the variation of temperature (equivalence ratio) at 1bar (Fig. 19) and then for the pressure variation up to 32 bar (Fig. 20) at constant temperature of 1850 K for the methane fuel. Interestingly, the model is able to predict the flame stabilisation at the vortex break down point i.e., close to the exit of the mixing tube, as per the design intent. The other two temperature cases are not usually different in terms of flame behaviour compared to that of the high-temperature case, at 1850 K.
This study has shown the influence of pressure and temperature has quite weak influence on the flame positioning indicating the good flame stability of the burner-combustor configuration for the fully pre-mixed fuel profile, representing the fuel gas operation mode.

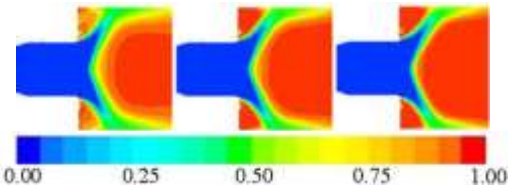

Figure 19: *Predictions of the AFSW reaction model in the F-2 configuration for three flame temperatures (1600 K, 1750 K and 1850 K) at 1bar. Shown are the contours of the reaction progress variable c*

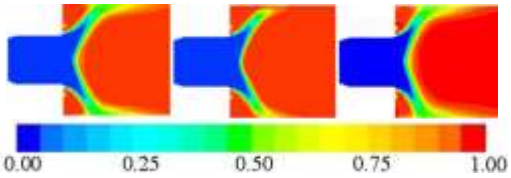

Figure 20: *Predictions of the AFSW model in the F-2 configuration for three operating pressures (1, 16 and 32 bar) at 1850 K. Shown are the contours of the reaction progress variable c.*

4.4.2 Influence of the Lewis Number on Flame Stability

The significance of this study sets a foot for investigation of dual fuels in gas turbines. The effect of *Le* is more predominant in higher molecular weight hydrocarbons (for e.g., diesel or octane) with *Le* hugely greater than one (whilst for lightest fuel hydrogen it is *Le*<<1). Here we focus for higher side of the Le values ranging from 1.0 to 2.6 as

Industrial Combustion
Journal of the International Flame Research Foundation
Article number 201618, June 2020
ISSN 2075-3071

shown in Table 5. It shows *Le* of 1.3 equivalent to that of propane/air mixture of equivalence ratio 0.5, and, the value of *Le* =2.6 equivalent to n-heptane of equivalence ratio~0.5.

Table 5: *Lewis number of n-heptane as a function of mixture fraction*

Fuel	CH_4	n-C_7H_{16} (mixture fraction 0.8)	n-C_7H_{16} (mixture fraction 0.5)	n-C_7H_{16} (mixture fraction 0.06)
Le	1.0	1.3	1.8	2.6

So, we actuate and see its consequence on the flame dynamics i.e. the position of the flame anchoring point (Fig. 21). For doubling *Le*, simulations show an ordinate decrease, by a factor of five in the reaction rate (and thus s_T), under other conditions unchanged. Physically, this amounts to anomalous flame drift into the combustor, a phase of undesired phenomenon in flame governance. Usually, the interface between burner-combustor is the acceptable flame anchoring point. For sake of completion, we infer that the reaction rate decreases as the rate of heat losses from the reaction zone exceeds the rate at which the reactant is transported into the reaction zone. Hence, the enthalpy and consequently the temperature decreases in the reaction zone while both increase in the preheat zone.

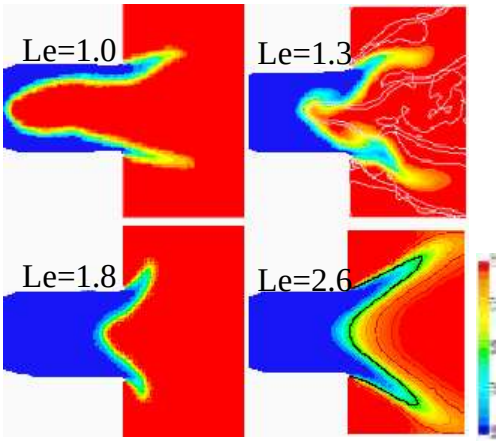

Figure 21: *Predictions of the AFSW model in the F-2 configuration 14 bar prevapourised premixed case by varying the Lewis number from 1.0 to 2.6. (contours of reaction progress variable, blue c=0 to red c=1)*

As evident, for *Le*= 1.3, despite s_T is only one-fifth of the 'strong' axial jet, flame drifting deep into the mixing tube is significant and penetrates further deep into the burner zone, albeit unstable. Such a movement may be explained following baroclinic push, discussed below.

4.4.3 Dynamics of Flame Propagation in Swirling Flows

The effect of baroclinic push is given as a function of $\nabla\frac{1}{\rho}\cdot\nabla p$ [36] where ρ is the density of the gaseous mixture, and p, the operating mean pressure inside the

Industrial Combustion
Journal of the International Flame Research Foundation
Article number 201618, June 2020
ISSN 2075-3071

chamber. In other words, the vorticity generation is a result of the existence of pressure gradients in a medium of varying density.

In specific to this flame scenario, coupling of the density gradient across the flame (occurring due to difference in unburned and burned gas velocities) and the radial mean pressure gradient in the unburnt swirling gas ahead of the flame results in generation of 'azimuthal vorticity', counter acting against the axial jet in the mixing tube. This is illustrated below for the flame simulated with Le=1.3. The azimuthal vorticity, which is shown marked with arrows around the vortex pair in Fig. 22, pushes the flame towards the upstream premixed unburnt gas. Upon increasing Le, the rate of heat losses from the reaction zone exceeds the rate at which the reactant is transported into the reaction zone. This further, decreases the temperature in the reaction zone and thereby the density gradient on the two major quantifiable flame quantities for model validation, flame brush and flame speed.

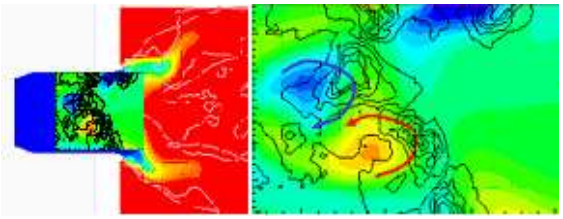

Figure 22: *Flame propagation mechanism: shown are the progress variable contours (left), inside the mixing tube; they are replaced with azimuthal vorticity (green part). The same part is zoomed for better visibility (right).*

This study signifies that the flame stability in gas turbine systems is a concern because flame positioning inside the chamber is sensitive to the mixing fields, temperature or equivalence ratio (and its fluctuations), as these can strongly effect the vortex break down phenomenon. Figs. 21 and 22 the vortex breakdown takes place deep inside the burner whilst it is desired to occur at the junction or outside the burner.

Conclusion

In this paper, algebraic flame surface wrinkling (AFSW) model application capabilities were verified for pressures as high as 10 bar and 32 bar, respectively, for the dump combustor and for a conical swirl burner respectively, for methane-air flames. Also, the importance of the Lewis number was quantified on the latter configuration for a given fuel profile. So, this study gives scope for extended investigations to mixed fuels. Also, emphasized in detail is the importance of molecular transport effects by close monitoring of flame dynamics of premixed turbulent combustion in a single burner gas turbine combustion system.

The quality of the closures in combination with the employed discretization schemes were estimated using LES index of quality (LES_IQ), as a quality assessment measure. The LES_IQ for cold and combusting flows were, respectively, 50–60% and 80% for the F-1 configuration. Also, the 'numerical' and 'model' error contributions on this geometry were separated following the Klein approach. This showed that the convolution of both errors resulted in a lower error due to their opposite signs.

In the complex swirl burner configuration, the propagation of the flame or the vortex breakdown point into the mixing tube was explained with baroclinic push i.e., coupling of the density gradient across the flame and the radial mean pressure gradient the unburnt swirling gas ahead of the flame. This coupling results in the generation of

azimuthal vorticity counter-acting against the axial jet in the mixing tube and thereby enhancing the flame propagation into the mixing tube.

Acknowledgement: This paper is based on the thesis of the first author Aluri Naresh Kumar.

References

1. Aluri, N.K., Pantangi, P. Muppala S.P.R. and Dinkelacker, F. *A Numerical Study Promoting Algebraic Models for the Lewis Number Effect in Atmospheric Turbulent Premixed Bunsen Flames.* Flow, Turbulence and Combustion, 2005. **75**: p. 149–172.
2. Aluri, N.K., Muppala, S.P.R. and Dinkelacker, F., *Substantiating a Fractal-based Algebraic Reaction Closure of Premixed Turbulent Combustion for High-Pressure and the Lewis Number Effects. .* Combustion and Flame, 2006. **145**: p. 663-674.
3. Griebel, P., Bombach, R., Inauen, A., Schären R. *Flame characteristics and turbulent flame speeds of turbulent, high-pressure, lean premixed methane/air flame.* in *ASME Turbo Expo.* 2005.
4. Lachaux, T., *PhD Thesis*. 2004, Universite d'Orleans, Orleans, France.
5. Griebel, P., Schaeren, R., Siewert,P. Bombach, R., Inauen, A., and Kreutner, W., *Flow field and structure of turbulent high-pressure premixed methane/air flames*, in *ASME Turbo Expo 2003, collocated with the 2003 International Joint Power Generation Conference* 2003, International Gas Turbine Institute: Atlanta, Georgia, USA. p. 301-310.
6. Biagioli, F., *Stabilization mechanism of turbulent premixed flames in strongly swirled flows.* Combustion Theory and Modelling., 2006. **10**(3): p. 389-412.
7. Wang, Z., Magi, V., & Abraham, J., *Turbulent Flame Speed Dependencies in Lean Methane-Air Mixtures under Engine Relevant Conditions.* Combustion and Flame, 2017. **180**: p. 53-62.
8. Chakraborty, N.a.C., RS., *Effects of Lewis number on flame surface density transport in turbulent premixed combustion. .* Combustion and Flame., 2011. **158**(9): p. 1768-1787.
9. Muppala S.P.R, Aluri, N.K., Dinkelacker, F., Leipertz, A., *Development of an algebraic reaction rate closure for the numerical calculation of turbulent premixed methane, ethylene, and propane/air flames for pressure up to 1.0 MPa.* Combust. and Flame, 2005. **140**: p. 257-266.
10. Ruan, S., Swaminathan, N., Isono, M., Saitoh, T., & Saitoh, K., *Simulation of Premixed Combustion with Varying Equivalence Ratio in Gas Turbine Combustor.* Journal of Propulsion and Power, 2015. **31**(3): p. 861–871.
11. Muppala, S.P.R., Vendra, C. Madhav Rao., and Aluri, Naresh K. , *Modelling and numerical simulation of dual fuel lean flames using local burning velocity and critical chemical timescale.* SAE International Journal of Engines, 2019. **12**: p. 373-385.
12. Burke, E.G., Güthe, F., Monaghan, R.F.D., *A comparison of turbulent flame speed correlations for hydrocarbon fuels at elevated pressures.* , in *ASME Turbo Expo*. 2016: Seoul, South Korea.
13. Bray, K.N.C., Libby, P.A. and Moss J.B. *Unified modeling approach for premixed turbulent combustion-part I: General formulation.* Combustion and Flame, 1985. **61**: p. 87-102.

14. Peters, N., *Turbulent Combustion.* . 2000: Cambridge University Press.
15. Damköhler, G., *Der Einfluss der Turbulenz auf die Flammengeschwindigkeit in Gasgemischen.* Zeitschrift für Elektrochemie und Angewandte Physikalische Chemie, 1940. **46**(11): p. 601-626.
16. Zimont, V.L. and Lipatnikov, A.N. *A numerical model of premixed turbulent combustion of gases. .* Chem. Phys. Reports, 1995. **14**(7): p. 993-1025.
17. Dinkelacker, F. Manickam, B. Muppala S. P.R., *Modelling and simulation of lean premixed turbulent methane/hydrogen/airflames with an effective lewis number approach.* Combust and Flame, 2011. **158**(9): p. 1742–9.
18. Lipatnikov, A.N. Chomiak, J. *Lewis Number Effects in Premixed Turbulent Combustion and Highly Perturbed Laminar Flames. .* Combusion Science and Technology, 1998. **137**: p. 277-298.
19. Muppala , S.P.R., Papalexandris, M.V. *A Modeling Approach for Hydrogen-Doped Lean Premixed Turbulent Combustion* in *ASME 2006 International Mechanical Engineering Congress and Exposition*. 2007: Chicago, Illinois, USA. p. 21-30.
20. Halter, F.C., Chauveau, C., Gökalp, I. , *Characterization of the effects of hydrogen addition in premixed methane/air flames.* Int. J. Hydrogen Energy, 2007. **32**: p. 2585-2592.
21. Jiang, Y.L., G. Li, H. Li, L. Zhang, G., *Experimental study on the turbulent premixed combustion characteristics of 70%H2/30%CO/air mixtures.* 2019. **44**(26): p. 14012-14022.
22. Zhou, R., Balusamy, S., Sweeney, M. S., Barlow, R. S., & Hochgreb, S., *Flow field measurements of a series of turbulent premixed and stratified methane/air flames. .* Combustion and Flame, 2013. **160**(10): p. 2017–2028.
23. Ashurst, W.M.T., *Flame propagation along a vortex: the baroclinic push. .* Combusion Science and Technology, 1996. **112**: p. 175-185.
24. Chomiak, J.and Hou, G, *A numerical study of large amplitude baroclinic instabilities of flames. .* Proceedings of the Combustion Institute, 1996. **26**: p. 883-889.
25. Shreekrishna, V.A., Lieuwen, T., *Flame Response to Equivalence Ratio Fluctuations — Relationship between Chemiluminescence and Heat Release.* International Journal of Spray and Combustion Dynamics, 2013. **5**(4): p. 329 – 358.
26. Benim, A.C.I., S. Meier, W. Joos, F. Wiedermann, A., *Numerical investigation of turbulent swirling flames with validation in a gas turbine model combustor. .* Applied Thermal Engineering, 2017. **110**: p. 202-212.
27. Celik, I.B., Cehreli, Z.N. and Yavuz.I, *Index of Resolution Quality for Large Eddy Simulations. .* ASME, Journal of Fluids Engineering, 2005. **127**: p. 949-958.
28. Klein, M., in *Private Communication*. 2005.
29. Meneveau, C., , 2005. Editors, J. Janicka et al. *Issues and Case Studies for Experimental Validation of LES in Incompressible Flows. .* in *Proceedings of the Conference on Quality Assessment of Unsteady Methods for Turbulent Combustion Prediction and Validation*. 2005. Department of Energy and Powerplant Technology, Tech. Univ. of Darmstadt, Germany.
30. Klein, M., *An attempt to assess the quality of large eddy simulations in the context of implicit filtering.* Flow Turbulence and Combustion, 2005. **75**: p. 131–147.

31. Soika, A., Dinkelacker, F. and Leipertz. A., *Pressure influence on the flame front curvature of turbulent premixed flames: comparison between experiment and theory.* Combustion and Flame, 2003. **132**(3): p. 451-462.
32. Kobayashi, H., Nakashima, T., Tamura, T., Maruta, K., Niioka, T. , *Turbulence measurements and Observations of Turbulent Flames at elevated pressures up to 3.0MPa.* Combust. and Flame, 1997. **108**: p. 104-117.
33. Yilmaz, B., Gökalp, I. , *Analysis of Turbulent Lean Premixed Methane–Air Flame Statistics at Elevated Pressures.* Energy Fuels, 2017. **31**(11): p. 12815-12822.
34. Fritz, J., *Flammenrückschlag durch verbrennungsinduziertes Wirbelaufplatzen*, in *Lehrstuhl für Thermodynamik.* 2003, Technische Universität München: München.
35. Schihl, P., Tasdemir, J. and Bryzik W., *Determination of Laminar Flame Speed of Diesel Fuel for Use in a Turbulent Flame Spread Premixed Combustion Model*, Transformational Science and Technology for the Current and Future Force 2006. Warren, MI USA.
36. Chomiak, J. and Nisbet, J.R. *Modeling variable density effects in turbulent flames-some basic considerations.* Combustion and Flame, 1995. **102**: p. 371-386.